Separation Science and Technology
Publication details, including instructions for authors and subscription information:
http://www.informaworld.com/smpp/title~content=t713708471

Adsorption of CO_2 on Zeolite 13X and Activated Carbon with Higher Surface Area

Zhijuan Zhang[a]; Wei Zhang[a]; Xiao Chen[a]; Qibin Xia[a]; Zhong Li[a]
[a] School of Chemistry and Chemical Engineering, South China University of Technology, Guangzhou, China

Online publication date: 04 March 2010

To cite this Article Zhang, Zhijuan , Zhang, Wei , Chen, Xiao , Xia, Qibin and Li, Zhong(2010) 'Adsorption of CO_2 on Zeolite 13X and Activated Carbon with Higher Surface Area', Separation Science and Technology, 45: 5, 710 — 719
To link to this Article: DOI: 10.1080/01496390903571192
URL: http://dx.doi.org/10.1080/01496390903571192

Separation Science and Technology, 45: 710–719, 2010

ISSN: 0149-6395 print/1520-5754 online
DOI: 10.1080/01496390903571192

Taylor & Francis
Taylor & Francis Group

Adsorption of CO_2 on Zeolite 13X and Activated Carbon with Higher Surface Area

Zhijuan Zhang, Wei Zhang, Xiao Chen, Qibin Xia, and Zhong Li
School of Chemistry and Chemical Engineering, South China University of Technology, Guangzhou, China

In this work, adsorption isotherms and adsorption kinetics of CO_2 on zeolite 13X and activated carbon with high surface area (AC-h) were studied. The adsorption isotherms and kinetic curves of CO_2 on the adsorbents were separately measured at 328 K, 318 K, 308 K, and 298 K and with a pressure range of 0–30 bar by means of the gravimetric adsorption method. The mass transfer constants and adsorption activation energy E_a of CO_2 on the adsorbents were estimated separately. Results showed that at very low pressure the amounts adsorbed of CO_2 on the zeolite 13X was higher than that on the AC-h, while at higher pressure, the amounts adsorbed of CO_2 on the AC-h was higher than that on the zeolite 13X since the AC-h has a larger surface area and a larger total pore volume compared to the zeolite 13X. The adsorption kinetics of CO_2 can be well described by the linear driving force (LDF) model. With the increase of temperature, the mass transfer constants of CO_2 adsorption on both samples increased. The adsorption activation energy E_a for CO_2 on the two adsorbents decreased with the increase of pressure. Furthermore, at low pressure the E_a for CO_2 adsorption on the zeolite 13X was slightly lower than that on the AC-h, while at higher pressure the E_a for CO_2 adsorption on the zeolite 13X was higher than that on the AC-h.

Keywords activated carbon with high surface area (Ac-h); activation energy; adsorption isotherms; adsorption kinetics; carbon dioxide removal; zeolite 13X

INTRODUCTION

Globally there is an increasing concern over the environmental impact of anthropogenic gas emissions, particularly carbon dioxide, with targets and taxes being implemented to decrease gas release to the atmosphere. Over the last century, rapid increase in atmospheric CO_2 concentration has resulted in global climate change and even more extreme climatic conditions (1–4). CO_2 emissions control could have significant social, economic and environmental impacts on the earth and humans (5–7).

Received 8 October 2009; accepted 6 December 2009.
Address correspondence to Zhong Li, School of Chemistry and Chemical Engineering, South China University of Technology, Guangzhou 510640, China. Fax: +86-20-87110608. E-mail: cezhli@scut.edu.cn

In the current stage, over 85 percent of the world energy demand is supplied by fossil fuels. Fossil-fueled power plants are responsible for roughly 40 percent of total CO_2 emissions, coal-fired plants being the main contributor (8). So the removal and recovery of CO_2 from coal-fired plants is considered to be the most effective way to reduce global CO_2 emissions from an energy point of view. Generally, there are three steps in CO_2 management: separation, transportation, and sequestration (9). Various strategies have been proposed to sequester CO_2, however, the key point for the sequestration is the removal of CO_2 by the gas separation process. In recent years, research works about CO_2 capture technologies including CO_2 absorption by aqueous ammonia (10–16), which was a typical technology but energy-consuming, cost-intensive (17–18), the removal of CO_2 emissions by pressure swing adsorption (PSA) (19–23), which proving to be a successful technology for the purificatiion and bulk separation of gas mixtures by either equilibrium or kinetic driving factors or temperature swing adsorption (TSA) (23,24) with porous materials, CO_2 separation by membrane (25–28) and ionic liquids (29) were reported. The capture or separation of CO_2 by adsorption will be one of the most important approaches in the commercial and industrial applications. Hence, the development of the adsorbent with high adsorption capacity, high selectivity, high thermal and chemical stability, and high adsorption rate is critical for a successful adsorptive process.

Nowadays, the sorption processes based on solid adsorbents are being actively pursued, especially using inorganic porous materials such as zeolite 13X, 4A, and activated carbon via physisorption in micropores for room and medium temperature application. Siriwardene et al. (30) studied the adsorption performance of molecular sieve 13X and activated carbon for CO_2 adsorption with volumetric methods in the pressure range of 0–20 bar. It was found that at low pressures (<25 psi) the adsorption capacity of the activated carbon for CO_2 was lower than that of the molecular sieve 13X, while at higher pressures (>25 psi) the activated carbon exhibited significantly higher

adsorption capacity of CO_2 compared to 13X. Lee et al. (31) studied the adsorption isotherms of CO_2 on zeolite 13X and zeolite 13X/activated carbon at low pressure range of 0–1.0 bar, and reported that the amount adsorbed of CO_2 on the zeolite 13X was higher than that on zeocarbon; however, the adsorption capacity of the two adsorbents became similar as the pressure increased. Cavenati et al. (32) studied the adsorption equilibrium of CO_2 on zeolite 13X at high pressures of 0–50 bar, and the zeolite 13X showed very strong and selective adsorption of CO_2. However, kinetic studies of CO_2 adsorption on porous adsorbents were rarely reported. Both adsorption equilibrium and kinetics are important parameters to value the adsorption performance of an adsorbent. Therefore, it is worth of studying the adsorption performance of CO_2 on the zeolite 13X and activated carbon with high surface area (AC-h).

The objective of this work is to study the CO_2 adsorption on the zeolite 13X and the activated carbon with high surface area(AC-h) at different temperatures. The adsorption isotherms and adsorption kinetic curves of CO_2 on the two adsorbents at different temperatures and pressures were separately measured. The adsorption rate coefficients and adsorption activation energies of CO_2 on the adsorbents would be estimated separately. The textural properties of the adsorbents were characterized by an Accelerated Surface Area and Porosimetry Apparatus (ASAP 2010). The effects of the pore size and surface area of the adsorbents on the CO_2 adsorption on the two adsorbents would be discussed and reported here.

EXPERIMENTAL

Materials and Instrumentation

Zeolite 13X (analytical grade), was purchased from the Chemical Plants of Tianjin (Tianjin, China). High surface area activated carbon was purchased from Tangshan Solid Carbon Co. Ltd of Hebei (Hebei, China), and its particle size was 300–400 mesh. Prior to use, the adsorbents were dried at 375 K for 24 h.

Maganetic suspension balance RUBOTHERM was used to measure the adsorption isotherms and kinetic curvers of CO_2 on an adsorbent, which is supplied by Germany. Its precision was 0.000001 g. ASAP 2010 sorptometer was supplied by Micrometrics Company, USA.

Nitrogen Adsorption Experiments

The specific surface area, pore volume, and average pore diameter of samples were measured by nitrogen adsorption at the liquid nitrogen temperature 77 K with the help of Micromeritics gas adsorption analyzer ASAP 2010 instruments. The zeolite 13X sample and the AC-h were separately degassed at 523 K for 8 h and 4 h in a vacuum environment before the nitrogen adsorption measurements. The BET surface area was calculated from the adsorption isotherms of N_2 using the standard Brunauer-Emmett-Teller (BET) equation. The pore size distributions (PSD) were determined using Density Funtional Theory (DFT) based on statistical mechanics. The specific surface area and the pore volume of the zeolite 13X and the AC-h were measured by the BET method. The average pore diameter $D_p = 4\,V_p/S_{BET}$ (assuming a cylindrical and a slit shape of pores, separately) was calculated from the BET surface area and pore volume.

CO_2 Adsorption Measurement

Determination of Adsorption Kinetic Curves of CO_2 on Adsorbents

The CO_2 adsorption kinetic experiments at 0.5 bar, 3.0 bar, 20.0 bar with different temperatures were obtained on a RUBOTHERM magnetic suspension balance. First, 1/3–1/2 (v% of sample container) adsorbent was introduced in the sample container, and the sample container was placed on the magnetic suspension balance located in the measuring cell. Second, the zeolite 13X and the AC-h were degassed at 523 K for 8 h and 4 h in a vacuum environment before the adsorption experiment start, and then, the weight of the sample zeolite 13X and the AC-h would be periodically recorded with the help of the magnetic suspension balance as the adsorption occurred. And the adsorption kinetic curves giving the amounts adsorbed of CO_2 on the two adsorbents as a function of time were measured. Third, the adsorption kinetic experiment ended when the weight of the sample got unvaried, meaning that the equilibrium had been achieved (the two adsorbents were saturated with CO_2). In order to get the adsorption kinetic curves for the adsorption of CO_2 on the zeolite 13X and the AC-h under the condition of different pressures, the adsorption kinetic experiments mentioned above of these two adsorbents were carried out separately at 0.5 bar, 3.0 bar, and 20.0 bar, and thus the adsorption kinetic curves at different pressures can be obtained.

Determination of Adsorption Isotherms of CO_2 on Adsorbents

The CO_2 adsorption-desorption isotherms at 298 K, 308 K, 318 K, 328 K were obtained on a RUBOTHERM magnetic suspension balance. The initial activation of the Zeolite 13X sample and the AC-h sample were carried out at 523 K for 10 h and 4 h in a vacuum environment, respectively. He (Ultra high purity, U-sung) was used as a purge gas in this study. The adsorption processes were carried out using high purity CO_2 (99.999%) gas. A feed flow rate of 100 mL/min and 30 mL/min, respectively, were controlled with a mass flow controller (MFC) to the sample chamber. Both adsorption and desorption experiments were conducted at the same temperature. The

temperature of the sorption chamber can be adjusted and maintained constant by an internal temperature sensor. And the pressure can be changed stepwise through the gas flow rate.

RESULTS AND DISCUSSION

Textural Properties

According to IUPAC classification, pores within porous materials can be divided into micropore (width less than 20 Å), mesopore (width between 20 and 500 Å), and macropore (width greater than 500 Å). Table 1 presents a summary of the textural parameters of the zeolite 13X and the AC-h. The data in Table 1 shows that the AC-h had a larger surface area and total pore volume in comparison with the zeolite 13X, while the average pore diameter of the zeolite 13X was lower than that of the AC-h.

Isotherms of CO_2 on the Zeolite 13X and the AC-H

Figures 1 and 2 show separately the adsorption isotherms of CO_2 on the zeolite 13X and the AC-h with different temperatures at the pressure from vacuum to 30.0 bar.

TABLE 1
Textural parameters of the zeolite 13X and AC-h

Sample	BET surface area [$m^2 \cdot g^{-1}$]	Average pore diameter [nm]	Total pore volume [$cm^3 \cdot g^{-1}$]
AC-h	2829	2.19	1.55
Zeolite 13X	164.3	1.00	0.21

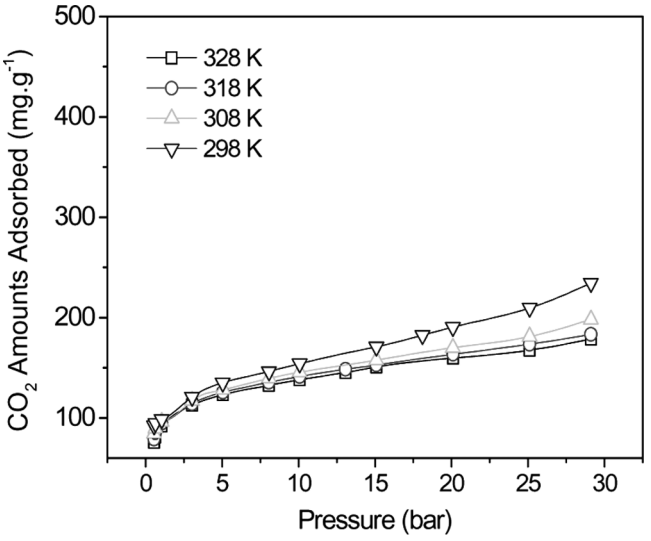

FIG. 1. CO_2 adsorption isotherms of the zeolite 13X at different temperatures.

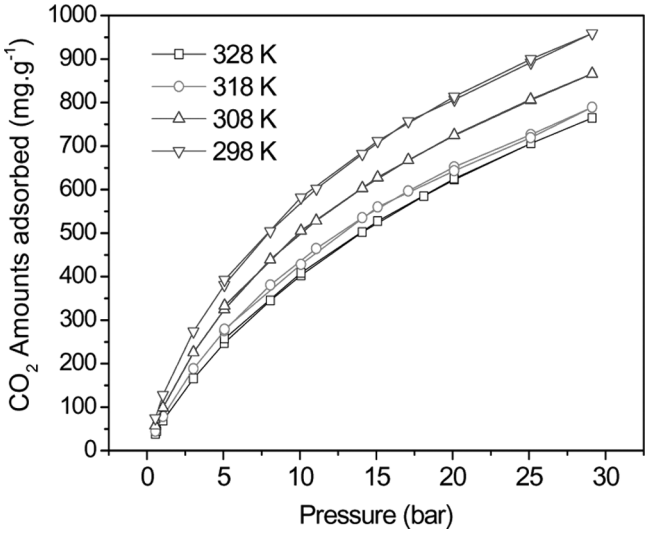

FIG. 2. CO_2 adsorption isotherms of the AC-h at different temperatures.

It can be seen that the amounts adsorbed of CO_2 on the zeolite 13X and the AC-h decreased with temperature, and the lower the temperature was, the larger the amounts adsorbed of CO_2 were. It meant that the adsorption of CO_2 is mainly physical adsorption.

Figures 3 and 4 give a comparison of the adsorption isotherms of CO_2 on the zeolite 13X and the AC-h at the temperatures of 298 K and 328 K, separately. It can be seen that at very low pressure the amounts adsorbed of CO_2 on the zeolite 13X was higher than that on the AC-h, which may be ascribed to its smaller pore diameter compared to the AC-h. With the increase of pressure, the adsorption

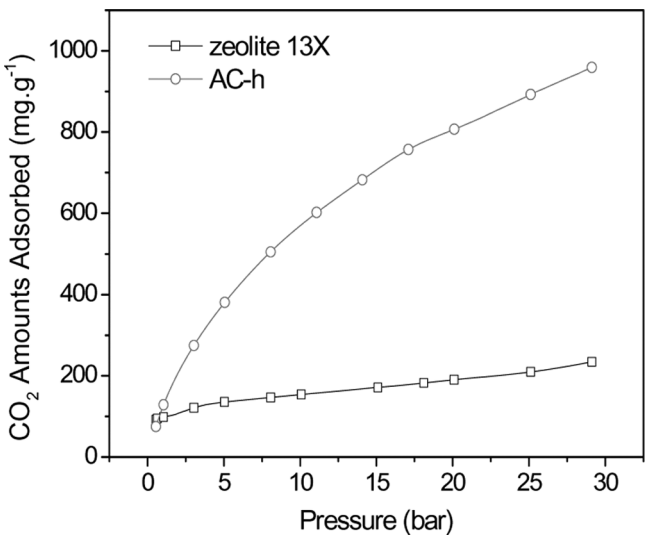

FIG. 3. CO_2 adsorption isotherms of two adsorbents at the temperature of 298 K.

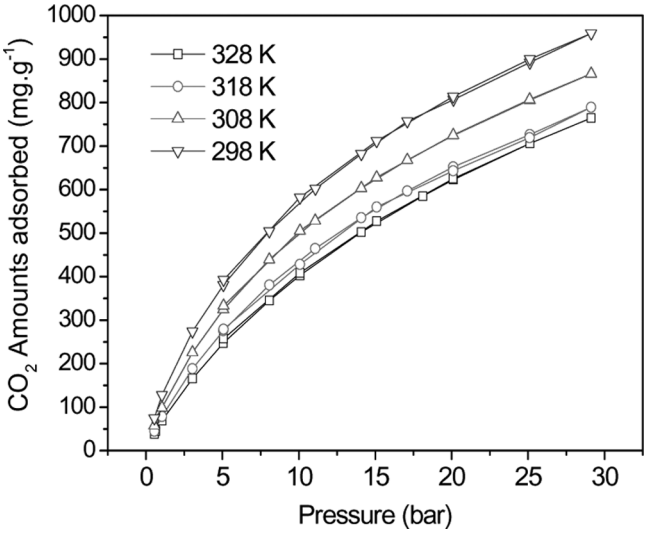

FIG. 4. CO_2 adsorption isotherms of two adsorbents at the temperature of 328 K.

capacity of the AC-h for CO_2 increased gradually and exceeded greatly that of the zeolite 13X since the AC-h has a larger surface area and a larger total pore volume compared to the zeolite 13X.

Figure 5 exhibits a comparison of the adsorption isotherms of CO_2 on the adsorbents at low pressure in the range of 0.5–2.0 bar. It can be seen that the amounts adsorbed of CO_2 on the zeolite 13X were higher than those on the AC-h at the pressure of 0–0.9 bar. It was because the pore diameter of the zeolite 13X was smaller than that of the AC-h. At lower pressure, the smaller the pore size was, the stronger the adsorption force field formed in the pore was, so the equilibrium amounts adsorbed of CO_2 was higher. However, when the pressure increased from 0.9 bar to 2.0 bar, the adsorption of CO_2 on the AC-h increased much faster due to its high surface area and total volume.

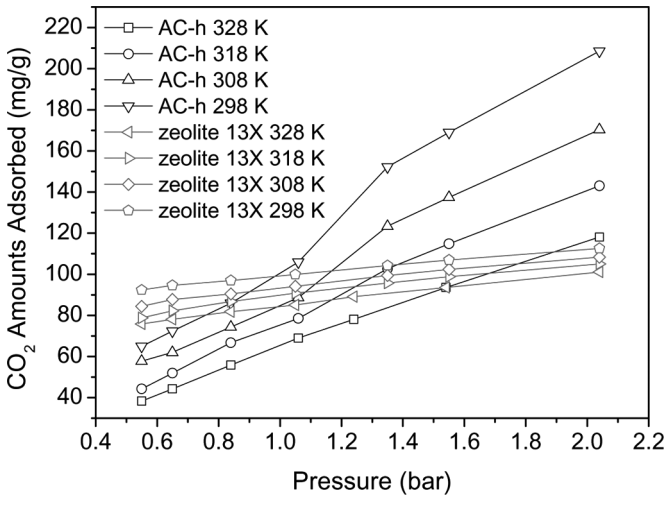

FIG. 5. CO_2 adsorption isotherms of the two samples at the pressure 0.5–2.0 bar with different temperatures.

In order to describe the CO_2 adsorption on these adsorbents clearly, the Langmuir equation was used to fit the isotherms. Langmuir derived the simple equation for the equilibrium adsorption isotherm as (33):

$$q_i = \frac{q_{\max} K P_i^*}{1 + K P_i^*} \tag{1}$$

Or

$$\frac{P^*}{q} = \frac{1}{q_{\max} K} + \frac{P^*}{q_{\max}} \tag{2}$$

Where q_i is the amount adsorbed in equilibrium with the concentration of adsorbate in gas phase (mg/g), q_{max} is the maximum adsorption amount (mg/g), P^* is the equilibrium pressure of the adsorbate in gas phase (bar), K is the equilibrium constant of adsorption. In the model, q_{max} and K can be calculated from the linear plots of p/q versus p.

Table 2 presents the parameters of Langmuir equation, their standard deviations $S.D.q_{max}$ and $S.D._K$, and the correlation coefficients (r^2) for the linear regression of the data presented in Figs. 1–2. The linear correlation of the data was good because the correlation coefficients r^2 were up to 0.98. It meant the adsorption behaviors of CO_2 on both adsorbents can be well described by the Langmuir adsorption equation. The data in Table 2 also indicated that the q_{max} values of CO_2 on the AC-h was far higher than that on the zeolite 13X, and the maximum adsorption capacity q_{max} of both adsorbents became lower with the increase of temperature, suggesting that the adsorption of CO_2 on both adsorbents was physical adsorption.

CO_2 Adsorption Kinetics

Figures 6–11 describe the adsorption kinetic curves of CO_2 on the two samples separately at 0.5, 2.0, and 20.0 bar with different temperatures. It can be seen that the amounts adsorbed of CO_2 on the adsorbents increased quickly during the initial adsorption stages, then increased slowly and finally reached equilibrium amounts. The higher the pressure of CO_2 was, the higher the equilibrium amount adsorbed of CO_2 on the adsorbent was.

In order to value or compare the adsorption rate of CO_2 on the two adsorbents, it is necessary to determine their mass transfer coefficients. Suppose M gram of adsorbent was suddenly placed in CO_2 flow. At time $t > 0$, the adsorption of CO_2 occurred, and the amount adsorbed, $q(t)$, of CO_2 on the adsorbent increased with time. The adsorption rate of CO_2 was assumed to follow first-order kinetics (linear driving force model) with the following equation used

TABLE 2
Parameters obtained by fitting of Langmuir equation and their standard deviations

Adsorbents	Temperatures [K]	Parameters for Langmuir model				
		q_{max} [mg/g]	S.D.q_{max} [mg/g]	K	S.D.$_K$	r^2
AC-h	328 K	1160.108	12.625	0.0583	0.0034	0.995
	318 K	1171.038	14.184	0.0633	0.0045	0.994
	308 K	1208.240	18.906	0.0766	0.0073	0.993
	298 K	1258.466	25.370	0.0927	0.0118	0.992
Zeolite 13X	328 K	184.162	16.920	0.566	0.0045	0.997
	318 K	186.220	14.520	0.673	0.0034	0.998
	308 K	200.401	22.375	0.471	0.0069	0.992
	298 K	235.849	14.951	0.378	0.0073	0.987

to describe the adsorption process (34–39):

$$\frac{\partial \bar{q}}{\partial t} = k_{eff}(q^* - q) \tag{3}$$

where k_{eff} is the mass transfer constant, q^* is the equilibrium amount adsorbed of CO_2 corresponding to the CO_2 concentration of gas phase at some temperature, and $q(t)$ is the CO_2 amount taken by the adsorbent at time t, which can be found out using the gravimetrical measurement method. From Eq. (3), integral equation was available as follows:

$$\ln\left(\frac{q^* - q}{q^*}\right) = -k_{eff}t \tag{4}$$

If the adsorption kinetic experiment of CO_2 is conducted at a certain pressure, the corresponding kinetic curve, $q(t) - t$ curve, could be obtained. After that, a plot of $-\ln(q^* - q)/q^*$ versus t will yield a line with slope k_{eff}. As a result, from the slope of the line, k_{eff} can be found out (40).

After adsorption kinetic curves of the zeolite 13X and the AC-h were available, as shown by Figs. 6–11, their mass transfer constants can be found out according to Eq. (4). Figure 12 and Fig. 13 show separately the plots of $\ln(q^* - q)/q^*$ versus time for CO_2 adsorption on the zeolite 13X and the AC-h. The plots were linearly fitted with correlation coefficients (r) more than 0.99 as shown in Figs. 12–13, indicating that the adsorption process of

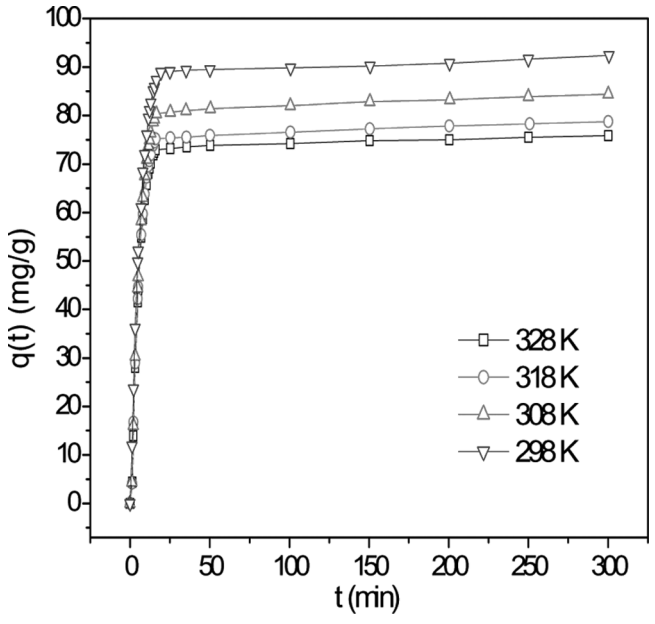

FIG. 6. Adsorption kinetics curves of CO_2 on zeolite 13X at 0.5 bar with different temperatures.

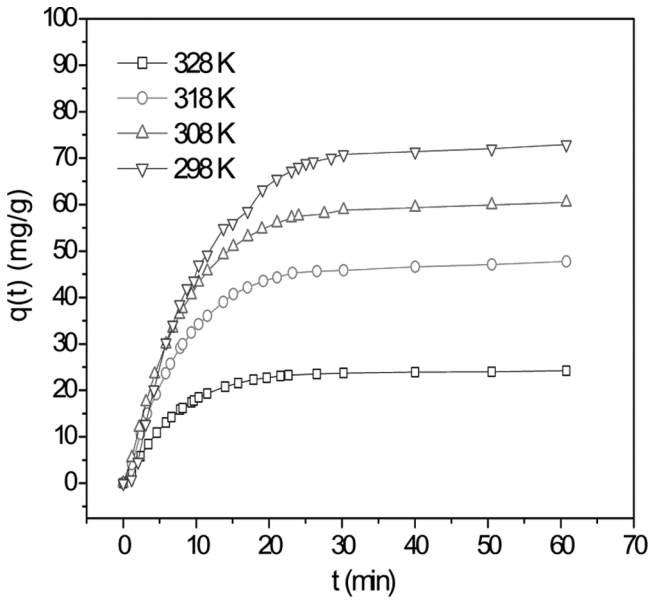

FIG. 7. Adsorption kinetics curves of CO_2 on the AC-h at 0.5 bar with different temperatures.

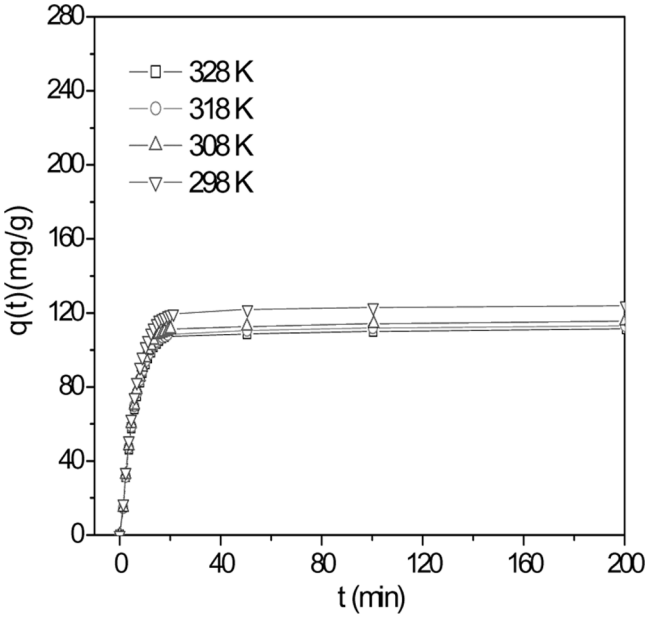

FIG. 8. Adsorption kinetics curves of CO_2 on the zeolite 13X at 3.0 bar with different temperatures.

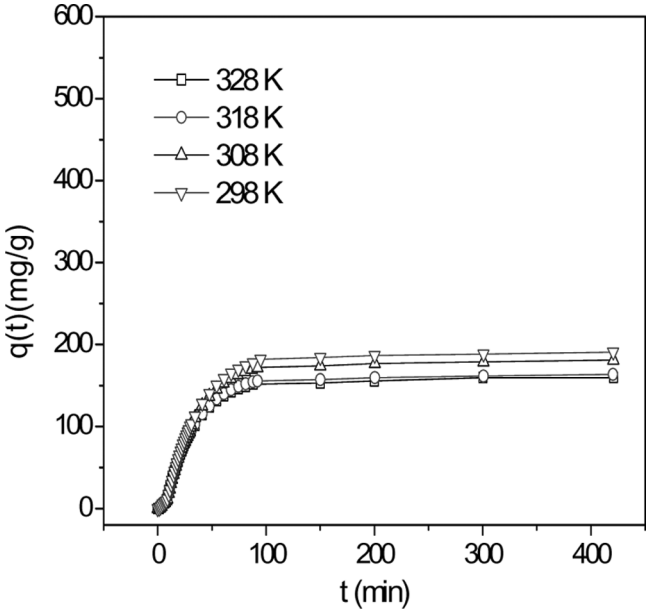

FIG. 10. Adsorption kinetics curves of CO_2 on the zeolite 13X at 20.0 bar with different temperatures.

CO_2 can be well described by Eq (3). From the slopes of these lines, the mass transfer constants of CO_2 on the two adsorbents were obtained, as listed in Table 3.

Table 3 lists the mass transfer coefficients of CO_2 diffusion within the adsorbents and their standard deviations $S.D._{13X}$ and $S.D._{AC\text{-}h}$. The data in Table 3 indicated that the mass transfer coefficients increased with the increase of temperature because the diffusion of CO_2 molecular became quicker with temperature, and decreased with the increase of pressure because the molecular diffusion resistance became larger with pressure. A comparison of the mass transfer coefficients k_{eff} of CO_2 on the zeolite 13X

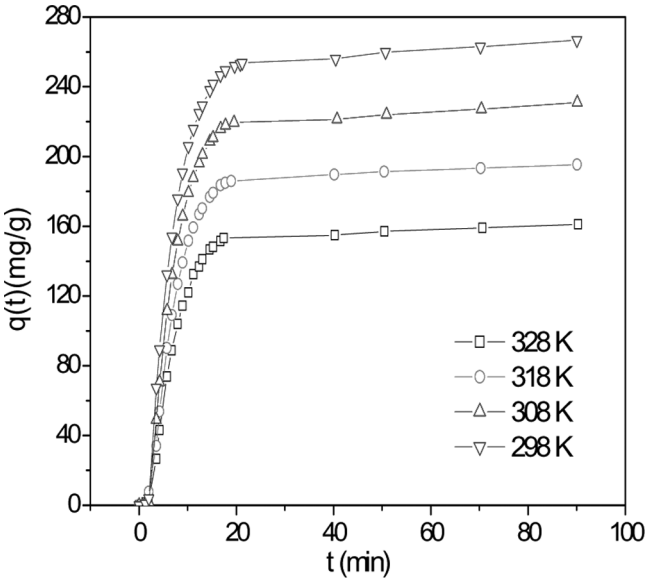

FIG. 9. Adsorption kinetics curves of CO_2 on the AC-h at 3.0 bar with different temperatures.

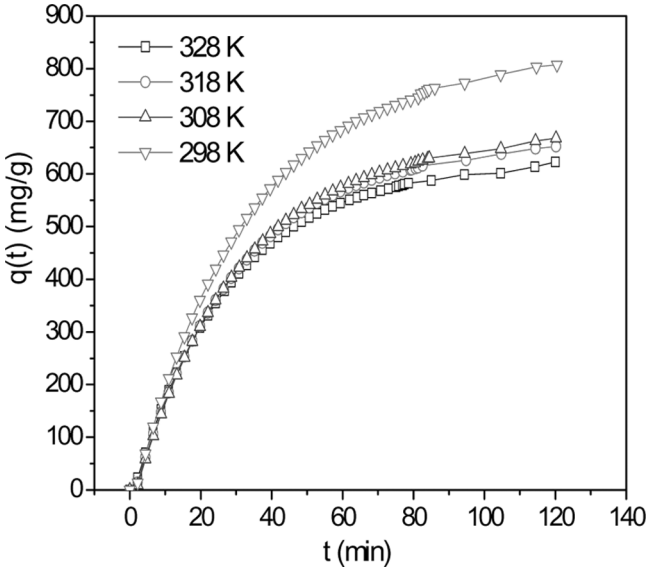

FIG. 11. Adsorption kinetics curves of CO_2 on the AC-h at 20.0 bar with different temperatures.

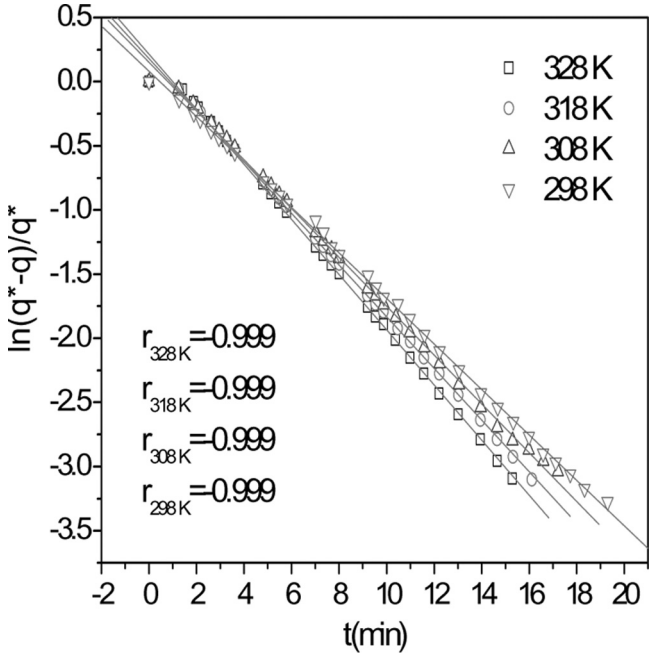

FIG. 12. Linear dependence between ln $(1 - q/q^*)$ and time for analysis of CO_2 adsorption kinetics on the zeolite 13X using the LDF model at 0.5 bar with different temperatures.

and the AC-h showed that at pressure of 0.5 bar, the k_{eff} of CO_2 on the zeolite 13X were higher than that on the AC-h. As the pressure increased further, the difference in mass transfer coefficients of CO_2 on both the zeolite 13X and the AC-h became smaller and smaller so that they were nearly the same at the pressure of 20.0 bar.

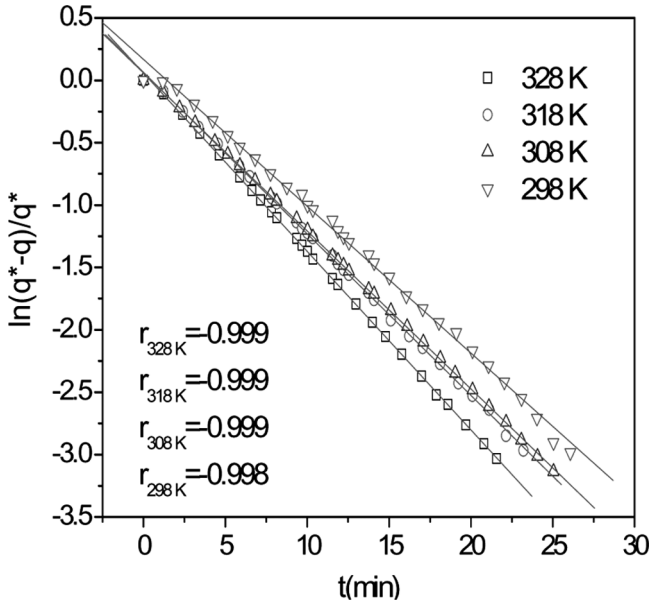

FIG. 13. Linear dependence between ln $(1 - q/q^*)$ and time for analysis of CO_2 adsorption kinetics on the AC-h using the LDF model at 0.5 bar with different temperatures.

After a series of the mass transfer coefficients k_{eff} of CO_2 at different temperature were available, the adsorption activation energy of CO_2 can be found out using the Arrhenius equation:

$$k_{eff} = A \exp(-E_a/RT) \tag{5}$$

where E_a, A and R refer to the Arrhenius activation energy, the Arrhenius factor and the gas constant, respectively. Eq. (5) can also be expressed as,

$$\ln k_{eff} = \ln A - E_a/RT \tag{6}$$

When $\ln k_{eff}$ is plotted to $(1/T)$ according to the data in Table 3, a straight line (slope $= -(E_a/R)$) can be obtained. Thus the adsorption activation energy E_a can be directly calculated from the slope of the straight line.

Figures 14 and 15 show the plots of $\ln k_{eff}$ versus the inverse temperature $(1/T)$ in an Arrhenius-type plot. The plots were linearly fitted with correlation coefficients (r^2) more than 0.95, showing a good linearity between $\ln k_{eff}$ and $1/T$. Thus the adsorption activation energies E_a were available from the slope of the straight line, which were listed in Table 4.

Table 4 lists the adsorption activation energies E_a of CO_2 on the two adsorbents at different pressures. It can be seen that the E_a decreased with the increase of pressure, which indicated that the adsorbate-adsorbent interaction potential of the two adsorbents for CO_2 was stronger at higher pressure. This is because, for physical adsorption, as the pressure increases, the adsorbate-adsorbent interaction potential of the adsorbent becomes stronger due to the increase of gaseous density, and hence the adsorption has a lower activation energy under higher pressure. In addition, it was noticed that at lower pressure of 0.5 bar, the E_a of CO_2 on the zeolite 13X was slightly lower than that on the AC-h, suggesting that the adsorbate-adsorbent interaction potential of the zeolite 13X for CO_2 was somewhat stronger compared to that of the AC-h. However, at the pressure higher than 3.0 bar, the adsorption activation energy E_a of CO_2 on the zeolite 13X was slightly higher than that on the AC-h, indicating that the adsorbate-adsorbent interaction potential of the AC-h for CO_2 was somewhat stronger in comparison with that of the zeolite 13X. The order of the adsorption activation energies of CO_2 on the two adsorbents at different pressures was nearly in consistent with that of the adsorption capacities of two adsorbents for CO_2 within a pressure range of 0.5–20.0 bar, as shown in Figs. 3–5.

TABLE 3
The mass transfer coefficients of CO_2 on the two materials and their standard deviations

		Mass transfer coefficients and their standard deviation k_{eff} [$\times 10^{-4}\,s^{-1}$]			
Pressure [bar]	Temperatures [K]	13X	S.D.$_{13X}$	AC-h	S.D.$_{AC\text{-}h}$
0.5	298 K	29.5	0.0468	19.6	0.0141
	308 K	31.7	0.0388	21.2	0.0204
	318 K	33.5	0.0414	22.6	0.0147
	328 K	35.8	0.0301	23.8	0.0503
3.0	298 K	25.3	0.1212	27.0	0.1027
	308 K	26.0	0.0717	29.5	0.0947
	318 K	29.2	0.0936	30.0	0.0719
	328 K	29.7	0.0669	31.5	0.0554
20.0	298 K	5.44	0.0653	5.53	0.1205
	308 K	5.63	0.0563	5.88	0.0841
	318 K	5.75	0.0595	5.99	0.0641
	328 K	6.07	0.0496	6.29	0.0480

CONCLUSIONS

The amounts adsorbed of CO_2 on the zeolite 13X at low pressure were higher than that on the AC-h due to the smaller pore size of the zeolite 13X. However, as the pressure increased further, the amounts adsorbed of CO_2 on the AC-h increased quickly, and when the pressures were up to 3.0 bar and 20.0 bar separately, the amounts adsorbed of CO_2 were up to 266.72 mg/g and 806.89 mg/g respectively which were much higher than that on the zeolite 13X. The adsorption kinetics of CO_2 can be well described by the linear driving force

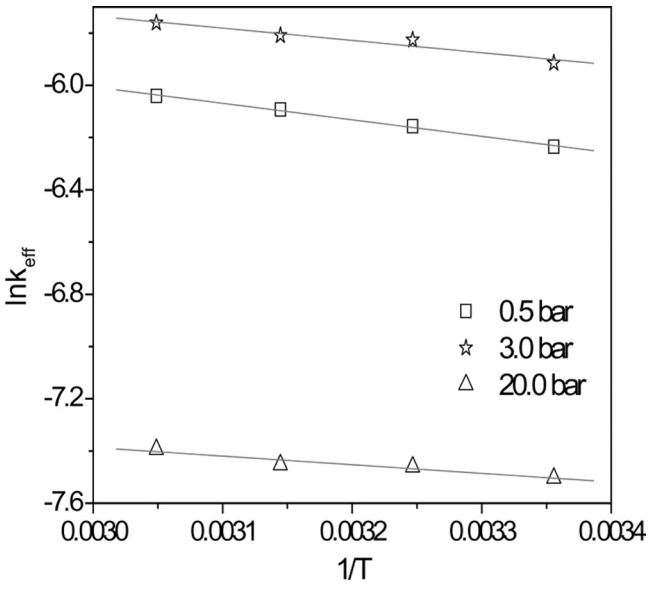

FIG. 14. Linear dependence between $\ln k_{eff}$ and 1/T for estimation of CO_2 adsorption activation energies on the zeolite 13X.

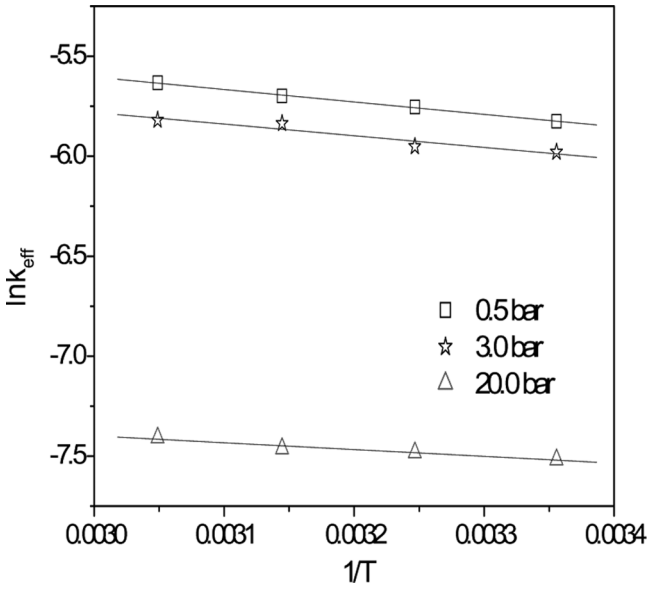

FIG. 15. Linear dependence between $\ln k_{eff}$ and 1/T for estimation of CO_2 adsorption activation energies on the AC-h.

TABLE 4
Adsorption activation energy, E_a, of CO_2 on the two adsorbents

	E_a [kJ/mol]		
Adsorbents	0.5 bar	3.0 bar	20.0 bar
AC-h	5.264	3.913	2.740
Zeolite 13X	5.167	4.854	2.831

(LDF) model. With the increase of temperature, the mass transfer constants of CO_2 adsorption on both samples increased. The adsorption activation energy E_a for CO_2 on the two adsorbents decreased with the increase of pressure. And at low pressure the E_a for CO_2 adsorption on the zeolite 13X was slightly lower than that on the AC-h, while at higher pressure the E_a for CO_2 adsorption on the AC-h was higher than that on the AC-h.

ACKNOWLEDGEMENTS

The authors would like to thank the National Natural Science Foundation of China (Grant No. 20336020).

REFERENCES

1. Cook, E.R.; Woodhouse, C.A.; Eakin, C.M.; Meko, D.M.; Stahle, D.W. (2004) Longterm aridity changes in the western United States. *Science*, 306: 1015–1018.
2. Meehl, G.A.; Tebaldi, C. (2004) More intense, more frequent, and longer lasting heat waves in the 21st century. *Science*, 305: 994–997.
3. Stott, P.A.; Stone, D.A.; Allen, M.R. (2004) Human contribution to the European heatwave of 2003. *Nature*, 432: 610–614.
4. King, D.A. (2004) Environment- Climate change science: Adapt, mitigate, or ignore? *Science*, 303: 176–177.
5. Lambeck, K.; Esat, T.M.; Potter, E.K. (2002) Links between climate and sea levels for the past three million years. *Nature*, 419: 199–206.
6. Pierce, J.L.; Meyer, G.A.; Jull, A.J.T. (2004) Fire-induced erosion and millennialscale climate change in northern ponderosa pine forests. *Nature*, 432: 87–90.
7. Westerling, A.L.; Hidalgo, H.G.; Cayan, D.R.; Swetnam, T.W. (2006) Warming and earlier spring increase western U.S. forest wildfire activity. *Science*, 313: 940–943.
8. Carapellucci, R.; Milazzo, A. (2003) Membrane systems for CO_2 capture and their integration with gas turbine plants. Proceedings of the Institution of Mechanical Engineers Part A. *Journal of Power and Energy*, 217: 505.
9. Holloway, S.; Pearce, J.M.; Hards, V.L.; Ohsumi, T.; Gale, J. (2007) Natural emissions of CO_2 from the geosphere and their bearing on the geological storage of carbon dioxide. *Energy*, 32: 1194–1201.
10. Chatti, R.; Bansiwal, A.K.; Thote, J.A.; Kumar, V.; Jadhav, P.; Lokhande, S.K.; Biniwale, R.B.; Labhsetwar, N.K.; Rayalu, S.S. (2009) Amine loaded zeolites for carbon dioxide capture: amine loading and adsorption studies. *Microporous and Mesoporous Materials*, 121: 84.
11. Yamasaki, A. (2003) An overview of CO_2 mitigation options for global warming- Emphasizing CO_2 sequestration options. *Journal of Chemical Engineering of Japan*, 36: 361.
12. Abanades, J.C.; Rubin, E.S.; Anthony, E.J. (2004) Sorbent cost and performance in CO_2 capture systems. *Industrial and Engineering Chemistry Research*, 43: 3462.
13. You, Jeong Kim; Jong, Kyun You; Won, Hi Hong; Kwang, Bok Yi; Chang, Hyun Ko; Jong-Nam, Kim (2008) Characteristics of CO_2 Absorption into Aqueous Ammonia. *Separation science and technology*, 43: 766.
14. Resnik, K.P.; Yeh, J.T.; Pennline, H.W. (2004) Aqua ammonia process for simultaneous removal of CO_2, SO_2 and NO_x. *International Journal of Environmental Technology and Management*, 4: 89–104.
15. Yeh, J.T.; Resnik, K.P.; Rygle, K.; Pennline, H.W. (2005) Semibatch absorption and regeneration studies for CO_2 capture by aqueous ammonia. *Fuel Processing Technology*, 86: 1533–1546.
16. Yang, H.Q.; Xu, Z.H.; Fan, M.H.; Gupta, R.; Slimane, R.B.; Bland, A.E.; Wright, I. (2008) Progress in carbon dioxide separation and capture: A review. *Journal of Environmental Sciences*, 20: 14–27.
17. Baker, R. (2002) Future Directions of Membrane Gas Separation Technology. *Industrial and Engineering Chemistry Research*, 41: 1393–1411.
18. Metz, A.; Davidson, O.; Coninck, H.; Loos, M.; Meyer, L. (2005) *IPCC Special Report; Carbon Dioxide Capture and Storage; International Panel on Climate Change*; Cambridge University Press: Cambridge, U.K.
19. Zou, Y.; Mata, V.; Rodrigues, A.E. (2000) Adsorption of carbon dioxide on basic alumina at high temperatures. *Journal of Chemical Engineering Data*, 45: 1093.
20. Gomes, V.G.; Yee, K.W.K. (2002) Pressure swing adsorption for carbon dioxide sequestration from exhaust gases. *Separation and Purification Technology*, 28: 161–171.
21. Zhao, X.X.; Xu, X.L.; Sun, L.B.; Zhang, L.L.; Liu, X.Q. (2009) Adsorption Behavior of Carbon Dioxide and Methane on $AlPO_4$-14: A Neutral Molecular Sieve. *Energy & Fuels*, 23: 1534.
22. Harlick, P.J.E.; Tezel, F.H. (2005) Equilibrium Analysis of Cyclic Adsorption Processes: CO_2 Working Capacities with NaY. *Separation Science and Technology*, 40: 2569–2591.
23. Chou, C.T.; Chen, C.Y. (2004) Carbon dioxide recovery by vacuum swing adsorption. *Seperation and Purification Technology*, 39: 51–65.
24. Douglas Aaron and Costas Tsouris. (2005) Separation of CO_2 from Flus Gas: A Review. *Separation Science and Technology*, 40: 328.
25. Powell, C.E.; Qiao, G.G. (2006) Polymeric CO_2/N_2 gas separation membranes for the capture of carbon dioxide from power plant flue gases. *Journal of Membrane Science*, 279: 2.
26. Luebke, D., Myers, C.; Pennline, H. (2006) Hybrid membranes for selective carbon dioxide separation from fuel gas. *Energy & Fuels*, 20: 1906.
27. Shekhawat, D.; Luebke, D.R.; Pennline, H.W. (2003) A review of carbon dioxide selective membranes – A topical teport. National Energy Technology Laboratory, United States Department of Energy.
28. Abidi, N.; Sivadea, A.; Bourret, D.; Larbot, A.; Boutevin, B.; Guida-Pietrasanta, F.; Ratsimihety, A. (2006) Surface modification of mesoporous membranes by fluoro-silane coupling reagent for CO_2 separation. *Journal of Membrane Science*, 270: 101.
29. Bara, J.E.; Carlisle, T.K.; Gabriel, C.J.; Camper, D.; Finotello, A.; Gin, D.L.; Noble, R.D. (2009) Guide to CO_2 separations in imidazolium-based room temperature ionic liquids. *Industrial and Engineering Chemistry Research*, 48: 2739.
30. Siriwardane, R.V.; Shen, M.S.; Fisher, E.P.; Poston, J.A. (2001) Adsorption of CO_2 on molecular sieves and activated carbon. *Energy & Fuels*, 15: 279–284.
31. Lee, J.S.; Kim, J.H.; Kim, J.T.; Suh, J.K.; Lee, J.M.; Lee, C.H. (2002) Adsorption equilibrium of CO2 on zeolite 13X and zeolite X/activated carbon composite. *Journal of Chemical and Engineering Data*, 47: 1237–1242.
32. Cavenati, S.; Grande, C.A.; Rodrigues, A.E. (2004) Adsorption equilibrium of methane, carbon dioxide, and nitrogen on zeolite 13X at high pressures. *Journal of Chemical and Engineering Data*, 49: 1095–1101.
33. Yu, M.X.; Li, Z.; Ji, Q.N.; Wang, S.W. (2009) Effect of thermal oxidation of activated carbon surface on its adsorption towards dibenzothiophene. *Chemical Engineering Journal*, 148: 242–247.
34. Crank, J. (1975) *The Mathematics of Diffusion*; Clarendon Press: Oxford.
35. Alsyouri, H.M.; Lin, J.Y.S. (2005) Gas diffusion and microstructural properties of ordered mesoporous silica fibers. *The Journal of Physical Chemistry B*, 109: 13623–13629.
36. Kennedy, L.J.; Vijaya, J.J.; Sekaran, G.; Kayalvizhi, K. (2007) Equilibrium, kinetic and thermodynamic studies on the adsorption of

m-cresol onto micro- and mesoporous carbon. *Journal of Hazardous Materials*, 149: 134–143.
37. Li, Z.; Yang, R.T. (1999) Concentration profile for linear driving force model for diffusion in a particle. *AIChE.J.*, 45: 196.
38. Liaw, C.H.; Wang, J.S.P.; Greenkorn, R.A.; Chao, K.C. (1979) Kinetics of fixed-bed adsorption: A new solution. *AIChE J.*, 25: 376.
39. Cossarutto, L.; Zimy, T.; Kaczmarczyk, J. (2001) Transport and sorption of water vapour in activated carbons. *Carbon*, 39: 2339–2346.
40. Zhao, Z.X.; LI, Z.; Xia, Q.B.; Xi, H.X. (2008) Swelling/Deswelling kinetics of PNIPAAm hydrogels synthesized by microwave irradiation. *Chemical Engineering Journal*, 142: 263–270.